BMC Ophthalmology

RESEARCH

Open Access

Axial elongation and the spatial distribution of white and dark without pressure in myopic eyes: insights from ultra-widefield imaging

Szy Yann Chan[1†], Chung Ting Pan[2†], Hai Ping Li[1] and Yue Guo Chen[1*]

Abstract

Background To explore the spatial distribution and associated factors of White and Dark Without Pressure lesions in myopic patients using ultra-widefield fundus imaging.

Methods This retrospective, observational study evaluated 2,940 eyes from 1,470 patients who underwent refractive surgery. Ultra-widefield fundus imaging was used to identify and map the distribution of white and dark without pressure lesions across 12 retinal sectors. Correlations between the incidence of these lesions, their location, axial length, and the number of affected sectors were analyzed.

Results White and dark without pressure lesions were present in 907 eyes (30.8%), with a significant association between increased axial length and higher incidence of white and dark without pressure ($P < 0.001$). Lesions were predominantly located in the temporal retina, specifically in the inferotemporal and superotemporal sectors. Longer axial length and younger age were both associated with a higher number of affected sectors and a more posterior localization of lesions.

Conclusion Axial elongation is significantly correlated with both the occurrence and posterior localization of white and dark without pressure lesions, as well as a higher number of affected sectors in myopic eyes. Ultra-widefield fundus imaging offers a comprehensive perspective on these retinal changes, providing valuable insights into the pathophysiology of white and dark without pressure.

Keywords White without pressure, Dark without pressure, Ultra-widefield fundus image, WWOP, DWOP

Background

White and Dark Without Pressure (WDWP) lesions, encompassing both White Without Pressure (WWOP) and Dark Without Pressure (DWOP), are retinal abnormalities predominantly observed in myopic individuals [1, 2]. WWOP is characterized by the presence of translucent white patches on the peripheral retina, whereas DWOP is identified by homogeneous dark brown or grayish areas, more frequently documented among individuals of African descent [3, 4]. These conditions are defined by distinctive retinal discolorations that occur independently of mechanical pressure and are often associated with peripheral retinal degeneration [5, 6]. The introduction of advanced imaging modalities, particularly ultra-widefield (UWF) fundus imaging, has significantly improved the detection and comprehensive evaluation of these lesions, facilitating

†Szy Yann Chan and Chung Ting Pan share the first authorship.

*Correspondence:
Yue Guo Chen
chenyueguo@263.net
[1] Department of Ophthalmology, Peking University, Beijing Key Laboratory of Restoration of Damaged Ocular Nerve, Peking University Third Hospital, 49 North Garden Rd, Haidian District, Beijing 100191, China
[2] Department of Ophthalmology, Peking University International Hospital, Beijing, China

a more detailed assessment of the retinal periphery [7–9].

Research have established a strong association between WDWP lesions and high myopia, driven by structural changes due to axial elongation [10, 11]. Although WDWP lesions are typically asymptomatic, their presence may indicate peripheral retinal structural vulnerability and may occasionally precede more serious pathologies such as retinal tears. Prior studies have suggested that these lesions may involve mechanical traction, retinal pigment epithelial disturbance, or early alterations at the vitreoretinal interface.

Increased axial length has been associated with mechanical stress (e.g., vitreoretinal traction, retinal thinning) and vascular stress (e.g., peripheral hypoperfusion) [12, 13], which may be particularly pronounced in the retinal periphery due to its structural and circulatory characteristics, and may contribute to the development of WDWP lesions [9, 12]. These stresses could lead to various forms of retinal degeneration and predispose the retina to other complications. Despite these findings, the precise mechanisms underlying the formation of WDWP lesions and their exact spatial distribution across different retinal sectors remain unclear. Furthermore,there is a notable lack of comprehensive studies utilizing advanced imaging modalities to fully characterize these lesions and understand their development over time.

Ultra-widefield fundus imaging offers a broad and detailed view of the retina, enhancing the ability to detect and quantify peripheral retinal lesions that might be overlooked with traditional imaging methods [7, 14–18]. This technique captures an expansive field of view, enabling the identification of lesions located in the far periphery of the retina. While previous studies utilized conventional imaging techniques, ultra-widefield fundus imaging provides an additional tool for exploring WDWP lesions. This advanced technology complements the clinical exam by offering a more comprehensive assessment of the retinal periphery.

This study aims to fill these gaps by employing UWF fundus imaging to investigate the spatial distribution of WDWP lesions in a cohort of patients undergoing refractive surgery. Additionally, it seeks to analyze the factors associated with the presence and distribution of WDWP lesions, with a particular focus on varying ocular axial lengths. By addressing these research gaps, we intend to provide deeper insights into the pathophysiology of WDWP leisions and its relationship with myopic changes.

Methods

Study population

This retrospective study reviewed patients who underwent refractive surgery at the Peking University Eye Center of Peking University Third Hospital between January 2020 and March 2021. The study included patients who had undergone laser-assisted in situ keratomileusis (LASIK), small incision lenticule extraction (SMILE), photorefractive keratecotomy (PRK), and implantable collamer lens (ICL) implantation procedures. The study adhered to the tenets of the Declaration of Helsinki and was approved by the Medical Ethics Committee of Peking University Third Hospital. All participants provided written informed consent prior to refractive surgery. The standard consent form included a statement that anonymized clinical data may be used for research purposes, which covered the retrospective analysis conducted in this study. Patients with fundus diseases, including a history of ocular surgery or trauma, uveitis, or corneal diseases that could affect refractive media, were excluded.Comprehensive preoperative ocular examinations were conducted, including uncorrected visual acuity (UCVA), best-corrected visual acuity (BCVA), intraocular pressure (IOP), slit-lamp biomicroscopy, dilated fundus examination, corneal topography, axial length (AL) measurement (IOL Master 500, Carl Zeiss Meditec AG, Germany), and ultra-widefield fundus photography (Optos, Marlborough, MA, USA).

Ultra-widefield fundus photography acquisition and quantification

All patients underwent mydriasis using 0.5% tropicamide and 0.5% phenylephrine before UWF fundus photography. Imaging was performed using a scanning laser ophthalmoscopy (SLO)-based system (Optos, Marlborough, MA, USA). Retinal specialists (S.Y.C, H.P.L, and the Retinal Specialist Group at Ophthalmology Center) reviewed preoperative dilated fundus examination records to exclude other retinal lesions and identify the presence of WDWP lesions. WDWP lesions were defined as distinct white or dark bands or patches on the retina, usually located in the peripheral retina, with continuous vascular course, differentiating it from other peripheral retinal degenerations or changes in the retinal pigment epithelium, such as congenital hypertrophy of the pigmented epithelium (CHRPE). Additionally, any peripheral retinal images that were blurred or out of focus, such as images where blood vessels lost focus during capture or where the image quality affected the measurement or evaluation of WDWP, were excluded. Other peripheral lesions, such as lattice degeneration or snail track lesions, were not analyzed due to inconsistent documentation and limited

visibility in retrospective imaging. Any discrepant cases were adjudicated by a panel of retinal experts, including two attending ophthalmologists, two associate chief physicians, and one chief physician from the Retinal Specialist Group at the Ophthalmology Center.

Ultra-widefield fundus images with WDWP were further analyzed using ImageJ software (National Institutes of Health; http://imagej.nih.gov/ij/). Since the macula is centrally located in the posterior pole (usually at the center of the image), the shortest distance from each WDWP lesion to the center of the fovea was measured using the shortest horizontal diameter of the optic disc (optic disc diameter, DD) as the unit of length. UWF images were divided into 12 sectors: SN1, SN2, SN3, IN4, IN5, IN6, IT7, IT8, IT9, ST10, ST11, and ST12 (Fig. 1) using the concentric rings map as a reference [19]. A sector was considered affected if any portion of a WDWP lesion overlapped with that sector. The presence of WDWP in each sector and the shortest distance from WDWP lesions to the macula were recorded. Measurements were conducted in the red channel for clearer disc boundary visualization and in the green channel for better WDWP boundary delineation.

Statistical analysis

All statistical analyses were conducted using SPSS for Mac OS version 29(IBM/SPSS, Armonk, NY, USA). Means and standard deviations (SD) were calculated for key variables.The axial length and age of the participants were each divided into four quartile groups. The Chi-Square test was employed to examine the relationship between axial length and the incidence of WDWP, controlling for the confounding effect of age. By stratifying the data based on age groups, we aimed to assess whether axial length independently influences the occurrence of WDWP. A *P*-value of less than 0.05 was considered statistically significant.

The distribution percentage of WDWP in the 12 sectors was calculated. Correlation analysis was performed to assess the relationship between axial length and the number of sectors affected by WDWP. Additionally, the correlation of axial length and age with the shortest distance from WDWP lesions to the macula in each sector was examined (Fig. 2).

To account for potential correlation between paired eyes from the same individual, generalized estimating equations (GEE) were applied. An exchangeable working correlation matrix was specified to model within-subject dependence.

All measurements were conducted by two experienced observers (S.Y.C. and C.T.P.). To ensure sufficient sample size and manage the dataset effectively while maintaining precision and reliability, random samples of 30 eyes were selected from each region, totaling 360 eyes. For intraobserver variability, each observer measured the distance in each sector twice, with re-examinations conducted at

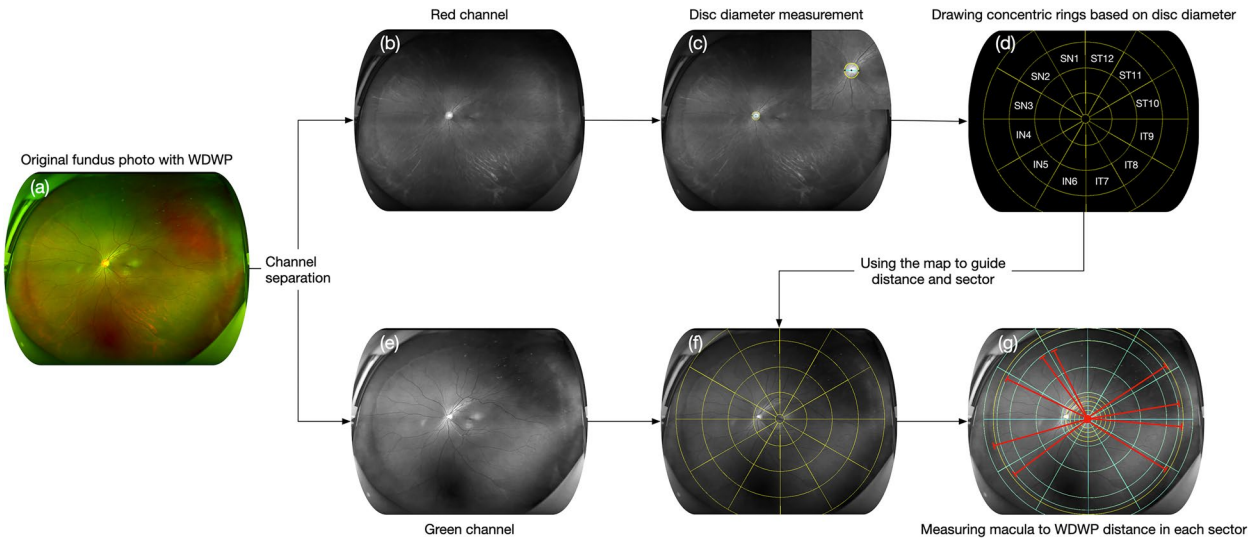

Fig. 1 Workflow for the measurement and analysis of WDWP distribution. This workflow demonstrates the process for accurately measuring and analyzing WDWP distribution using separated color channels and a structured mapping approach. The process begins with the original fundus image showing WDWP lesions (**a**). The image is separated into red (**b**) and green (**c**) color channels. In the red channel, the optic disc diameter is measured (blue line in c) and used to create concentric rings (**d**). In the green channel, the concentric rings map serves as a reference (**f**-**g**) for measuring the distance from the macula to WDWP lesions across different retinal sectors, as indicated by the red line in (**g**). The ring shown in this figure is for illustrative purposes only and does not represent the full extent of the analyzed area. All lesions within the visible peripheral retina were included in the analysis

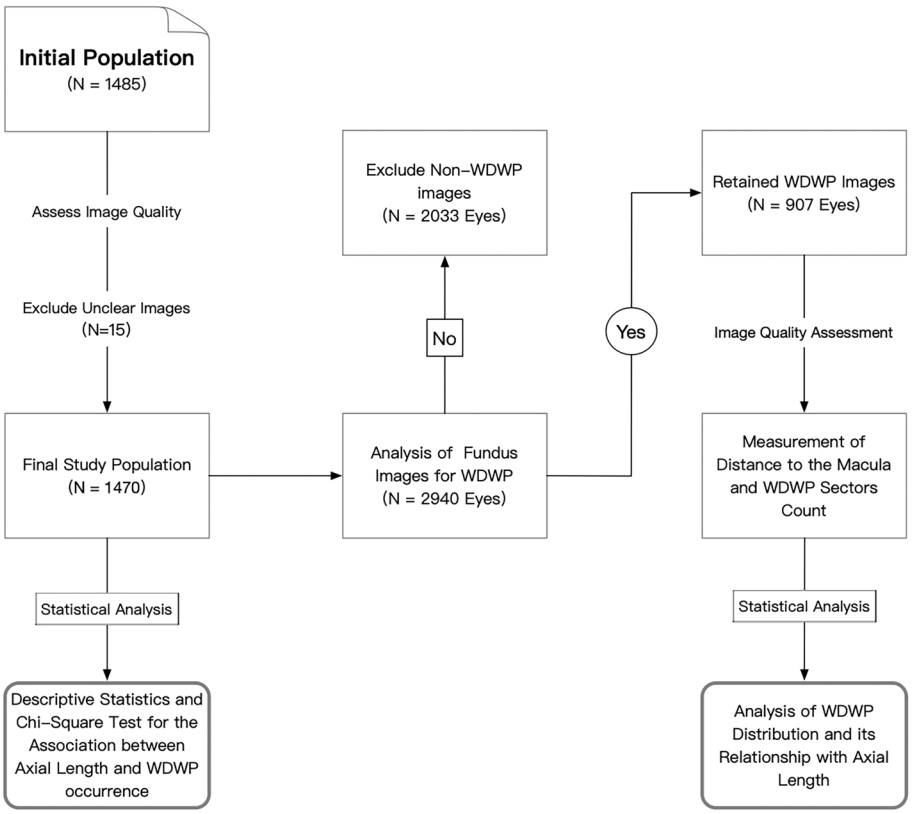

Fig. 2 Flowchart of Study Population and Image Analysis Process. This flowchart illustrates the selection and analysis of fundus images. From an initial 1,485 myopic patients, 15 were excluded due to unclear or missing images, leaving 1,470 for analysis. Images without WDWP (2,033 eyes) were excluded, while 907 eyes with WDWP were further analyzed. The images were assessed for distance to the macula and WDWP sector count, with statistical analyses exploring factors and the relationship between WDWP distribution and axial length

intervals of 1–2 weeks. The intraclass correlation coefficient (ICC) and coefficient of variation were calculated to assess the reliability of these measurements. To evaluate interobserver consistency, Lin's concordance correlation coefficient and Bland–Altman plots were employed.

Results

A total of 1485 patients were initially included in the study. After excluding 15 patients due to missing or unclear images, 2940 eyes of 1470 patients (708 males) with a mean age of 26.7 ± 7.2 years (range: 17–52 years) were analyzed. The mean axial length was 25.8 ± 1.2 mm (range: 21.1–31.7 mm). WDWP was identified in 907 eyes (30.8 ± 0.9%) with 203 patients having unilateral and 352 having bilateral involvement. WDWP was not found in 2033 eyes (69 ± 0.8%). The design and workflow of the study population are illustrated in Fig. 2.

A Chi-Square test of independence revealed a statistically significant association between axial length (AL) quartiles and WDWP occurrence across all age groups ($P < 0.001$). In each age group, higher AL quartiles corresponded to an increased occurrence of WDWP, with the fourth quartile consistently showing the highest WDWP rates (43.6% to 61.7%)(Table 1) (Fig. 3).

The GEE model indicated that both longer axial length and younger age were significantly associated with the presence of WDWP lesions. Specifically, each 1-mm increase in axial length was associated with greater odds of WDWP (B = 0.818, 95% CI: 0.697 to 0.939, $p < 0.001$), while each additional year of age was associated with lower odds (B = –0.035, 95% CI: –0.052 to –0.018, $p < 0.001$), after adjusting for inter-eye correlation.

In the 907 eyes with WDWP, a total of 3624 WDWP sectors were identified. The highest frequencies were in the IT9 (19.1 ± 0.7%) and ST10 (18.4 ± 0.6%) sectors, followed by IT8 (12.8 ± 0.6%) and ST11 (10.4 ± 0.5%). This indicates that WDWP is predominantly located in the temporal retina, from the superotemporal to the inferotemporal regions (Table 2).

Further analysis revealed that the number of sectors affected by WDWP was significantly associated with both younger age ($P < 0.001$) and longer axial length ($P < 0.001$). After adjusting for disc diameter, there was a significant negative correlation between

Table 1 Association between Axial Length and WDWP Occurrence by Age Group. This table shows the relationship between axial length (AL) quartiles and the occurrence of White and Dark Without Pressure (WDWP) lesions across age groups. Statistical significance is indicated by Pearson Chi-Square (χ^2) values and *p*-values, highlighting a significant association between longer AL and higher WDWP occurrence ($P < 0.001$)

Age Group (years)	AL Quartile (mm)	Count (N)	WDWP Occurrence (%)	Expectied Count (N)	Pearson Chi-Square (χ^2)	*P* Value
< 26	Q1 (21.1–25.0)	137	12.4	88.4	117.868	< 0.001*
	Q2 (25.0–25.8)	180	16.7	116.1		
	Q3 (25.8–26.6)	204	41.7	131.6		
	Q4 (26.6–31.7)	223	59.2	143.9		
26–29	Q1 (21.1–25.0)	160	8.8	107.6	110.554	< 0.001*
	Q2 (25.0–25.8)	178	24.2	119.7		
	Q3 (25.8–26.6)	214	36.0	143.9		
	Q4 (26.6–31.7)	162	61.7	108.9		
29–38	Q1 (21.1–25.0)	222	13.5	148.7	103.506	< 0.001*
	Q2 (25.0–25.8)	198	24.7	132.6		
	Q3 (25.8–26.6)	166	41.0	111.2		
	Q4 (26.6–31.7)	180	58.9	120.4		
> 38	Q1 (21.1–25.0)	211	12.3	165.0	57.352	< 0.001*
	Q2 (25.0–25.8)	183	12.0	143.1		
	Q3 (25.8–26.6)	154	26.0	120.4		
	Q4 (26.6–31.7)	168	43.6	131.4		
Overall	Q1-Q4	2940			385.670	< 0.001*

* Statistical Significance

AL axial length, *WDWP* white and dark without pressure

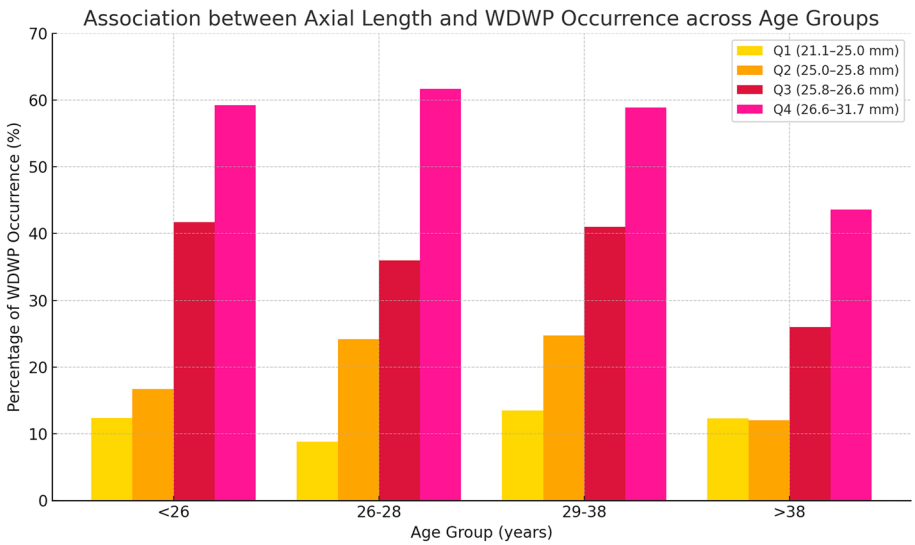

Fig. 3 Association between Axial Length (AL), Age Group, and WDWP Occurrence. This graph shows the percentage of WDWP occurrence across different age groups and AL quartiles. Higher AL quartiles are consistently linked with greater WDWP occurrence

axial length and the measured distance from WDWP lesions to the macula in most sectors, except SN1, SN2, and ST12. Additionally, in sectors SN3, IT8, IT9, and ST10, the distance from WDWP lesions to the macula was positively correlated with age (Table 2). This indicates that younger age and longer axial length both increase the number of affected sectors, while longer axial length tends to move WDWP lesions closer to

Table 2 WDWP Distribution and Correlation with Axial Length and Age. This table illustrates the distribution of WDWP across different retinal sectors, the mean shortest distance from WDWP to the macula measured in disc diameters (DD), and their associations with axial length and age. The table includes *p*-values, standardized coefficients (Beta), unstandardized coefficients (B), and 95% confidence intervals

Sector	Sectors Involved(%)	Mean ± SD (DD)	Associations with Axial Length (after Adjusting for DD)				Associations with Age (after Adjusting for DD)			
			P Value	Beta	B	95% Confidence Interval	*P* Value	Beta	B	95% Confidence Interval
SN1	67 (1.9 ± 0.2)	8.21 ± 1.96	0.160	-0.16	-0.28	-0.67, 0.12	0.972	0.004	0.001	-0.07, 0.07
SN2	90 (2.5 ± 0.3)	9.82 ± 2.03	0.320	-0.10	-0.19	-0.56, 0.19	0.739	0.03	0.01	-0.06, 0.08
SN3	204 (5.6 ± 0.4)	11.14 ± 2.23	0.001*	-0.20	-0.38	-0.59, -0.17	0.003*	0.18	0.06	0.02, 0.11
IN4	239 (6.6 ± 0.4)	11.05 ± 2.30	< 0.001*	-0.19	-0.38	-0.59, -0.17	0.112	0.09	0.03	-0.01, 0.07
IN5	203 (5.6 ± 0.4)	9.75 ± 2.06	0.003*	-0.20	-0.37	-0.61, -0.13	0.776	0.02	0.01	-0.04, 0.05
IN6	243 (6.7 ± 0.4)	8.41 ± 2.05	0.017*	-0.14	-0.29	-0.52, -0.05	0.492	0.04	0.02	-0.03, 0.06
IT7	283 (7.8 ± 0.4)	8.40 ± 2.14	< 0.001*	-0.24	-0.48	-0.69, -0.27	0.503	0.04	0.01	-0.03, 0.06
IT8	465 (12.8 ± 0.6)	9.90 ± 2.30	< 0.001*	-0.30	-0.62	-0.78, -0.45	0.011*	0.10	0.04	0.01, 0.07
IT9	692 (19.1 ± 0.7)	10.36 ± 2.11	< 0.001*	-0.29	-0.54	-0.66, -0.42	0.017*	0.08	0.03	0.01, 0.05
ST10	665 (18.4 ± 0.6)	10.52 ± 2.06	< 0.001*	-0.26	-0.47	-0.59, -0.36	0.016*	0.08	0.03	0.01, 0.05
ST11	378 (10.4 ± 0.5)	10.55 ± 2.31	< 0.001*	-0.33	-0.64	-0.80, -0.48	0.140	0.06	0.03	-0.01, 0.06
ST12	95 (2.6 ± 0.3)	9.11 ± 2.19	0.310	-0.09	-0.17	-0.50, 0.16	0.810	-0.02	-0.01	-0.07, 0.06
Total	3624 (100)									

* Statistical Significance

WDWP white and dark without pressure, *DD* disc diameter

Beta Standardized Coefficient, *B* Unstandardized Coefficient

the posterior region of the globe, especially in younger patients.

The measurement of the distance from WDWP to the macula showed an intraclass correlation coefficient (ICC) of 1.000 ($P < 0.001$), signifying excellent intraobserver consistency. The average coefficient of variation was 24.47% ± 0.03%. For interobserver variability, the concordance correlation coefficient was calculated as $r = 0.996$, indicating strong agreement between examiners. The Bland–Altman plot showed that 5.8% (21/360) of the measurements fell outside the 95% limits of agreement, reinforcing the high level of interobserver reliability.

Discussion

In this study, we investigated the incidence and characteristics of WDWP lesions in a cohort of patients undergoing refractive surgery, using UWF imaging to accurately quantify the spatial distribution and correlates of WDWP lesions. Our findings demonstrate a significant association between longer axial length and the presence of WDWP lesions, corroborating previous studies that link myopic changes with peripheral retinal abnormalities [1, 2, 11]. In our study, the incidence of WDWP in myopic patients was approximately 31%, consistent with earlier research findings [8].

Pearson Chi-square analysis revealed a positive association between axial length and WDWP prevalence, potentially reflecting cumulative mechanical and vascular stress on the peripheral retina in eyes with greater elongation [20]. Previous studies [1, 11, 21] have shown that younger age is associated with the occurrence of WDWP, indicating that younger individuals are more prone to developing these lesions. In our study, there appears to be a slight decline in WDWP incidence with increasing age, although this trend is not very pronounced (Fig. 3). This may reflect a cohort effect, in which younger individuals undergoing refractive surgery tend to have earlier-onset or more rapidly progressive myopia, resulting in longer axial length despite their age. Further analysis with larger sample sizes is required to clarify this observation.

The regional analysis indicated a predilection of WDWP lesions in the inferotemporal and superotemporal quadrants, with IT9 and ST10 sectors exhibiting the highest frequencies, which is consistent with previous research findings [1, 22–24]. This pattern may reflect regional anatomical and biomechanical vulnerabilities in the inferotemporal and superotemporal retina, where the retinal tissue is thinner, structural support is weaker, and the retina is more exposed to horizontal shearing forces and peripheral vitreoretinal traction during ocular movements. Our observation that WDWP lesions tend

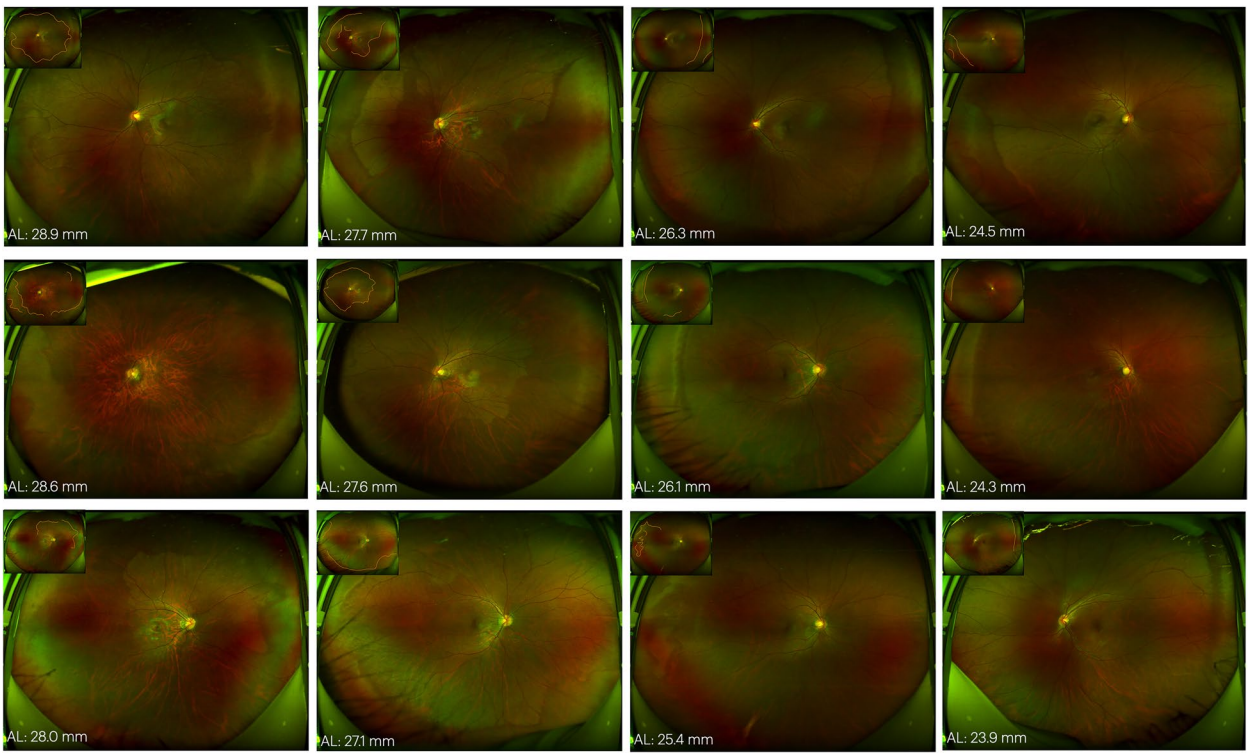

Fig. 4 Ultra-widefield images of white and dark without pressure (WDWP) lesions. With increasing axial elongation, WDWP lesions are located closer to the posterior pole, extending from the peripheral retina, and involving more retinal sectors. The inset in the upper-left corner of each image highlights the location of WDWP lesions, marked by orange curved lines. The axial length (AL) of each eye is shown in the lower-left corner of each image

to locate posteriorly with increasing axial length (Fig. 4) further supports the notion that axial elongation exacerbates peripheral retinal stress.

The etiology of WDWP remains unclear. However, our study's results suggest that as axial length increases, the vitreous may exert greater axial tractional forces on the retina. These forces appear to be more pronounced near the posterior pole compared to the peripheral retina, which could account for the more posterior localization of WDWP lesions in eyes with longer axial lengths. This suggests that in more myopic eyes, WDWP lesions are more likely to be found closer to the posterior pole (Fig. 5). This hypothesis indicates that the axial component of vitreous traction significantly influences the progression and distribution of WDWP lesions. These forces may exert stress on specific retinal regions, altering the mechanical environment of the retinal interface compared to surrounding areas, leading to changes in color and microstructure that manifest as WDWP lesions. Interestingly, age may also play a role in certain sectors, with younger individuals showing WDWP closer to the posterior pole. Younger patients may have a denser vitreous, which, along with increasing axial length, could contribute to stronger vitreous traction on the retina, potentially leading to a broader distribution of WDWP lesions.

Moreover, Orlin et al. [25] used ultra-widefield fluorescein angiography (UWFA) to evaluate eyes with WWOP and found that these eyes exhibited specific peripheral vascular patterns. The study identified three common UWFA patterns, with eyes exhibiting WWOP showing more frequent peripheral vascular abnormalities compared to those without WWOP. This aligns with our findings of higher lesion frequencies in the temporal quadrants and supports the hypothesis that fluorescein leakage or staining in regions of WWOP could be related to vitreous traction on the retina. Similar observations are documented in fluorescein angiography of patients with epiretinal membranes (ERM), where vascular leakage results from mechanical forces [26, 27].

Our findings are consistent with those reported by Yu et al. [11], who observed that longer axial length and more severe myopia are risk factors for both WWOP and DWOP. Moreover, their study noted reduced vessel density and retinal thickness in eyes with DWOP, providing morphological evidence of the structural changes associated with these conditions. Additionally, Some authors [3, 28] described changes in outer retinal reflectivity

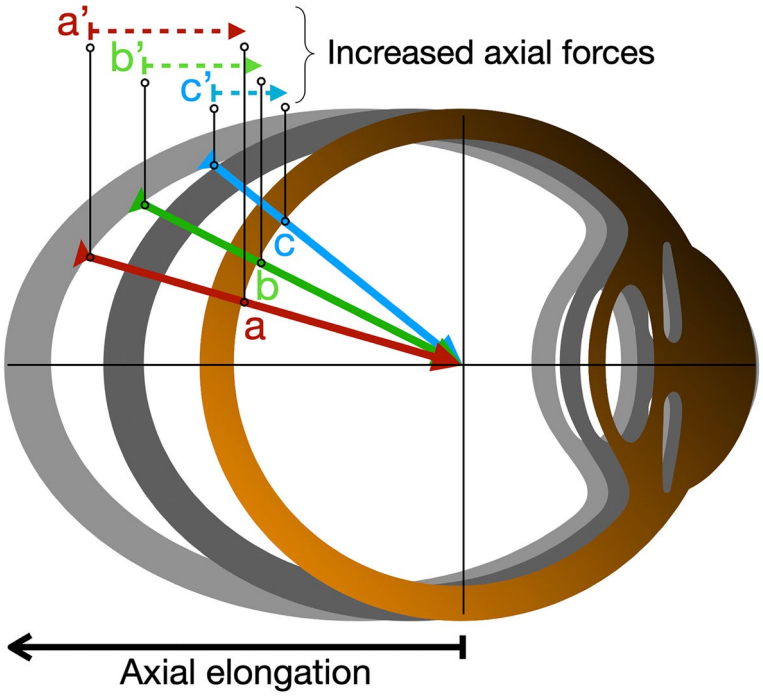

Fig. 5 Axial Traction Changes and WDWP Lesion Variation. This schematic illustration represents a conceptual hypothesis derived from our data, showing how axial traction forces at different retinal locations may change with increasing axial length. Solid lines (red, green, blue) represent initial traction at points a, b, and c, respectively. As axial length increases, these points shift posteriorly (a' to a, b' to b, c' to c). Retinal regions closer to the posterior pole (e.g., a') are hypothesized to experience greater increases in axial traction compared to more peripheral areas (e.g., b', c'). Dashed lines indicate the additional traction induced by elongation. This conceptual model may explain the observed posterior shift of WDWP lesions in eyes with longer axial lengths

associated with WDWP lesions, highlighting the importance of advanced imaging techniques in identifying and characterizing these abnormalities. Furthermore, the study by Nagpal et al. [29] suggested a potential transient nature of DWOP lesions observed primarily in patients with systemic conditions like sickle cell hemoglobinopathies and systemic hypertension. Although the exact cause remains unknown, these observations support the hypothesis of mechanical and vascular factors playing a role in WDWP development.

To our knowledge, this is the first study to conduct a large-scale evaluation of a myopic population and systematically assess eyes with WDWP and their spatial distribution. Utilizing advanced UWF imaging systems and a statistical approach, we aim to elucidate the potential pathogenesis of WDWP.

Several limitations warrant consideration. First, the cross-sectional design precludes causal inferences, and the study's focus on a refractive surgery population may limit generalizability. The sample was derived from a single hospital and primarily consisted of patients undergoing refractive surgery, which may not be representative of the general myopic population. Future studies should include a more diverse and larger population sample to improve generalizability. Second, the retrospective nature of the study means that the data collected may be subject to biases and inaccuracies related to past records and image quality. Prospective studies are needed to verify these findings. Third, the technique and approach to evaluating WDWP lesions require further validation, as UWF images are known to have distortion near the peripheral retina, which may introduce measurement errors [16, 17]. A previous study [17] have suggested that the enlargement factor of peripheral images remains consistent despite varying axial lengths, and the newer software (V2 Vantage Pro, Optos) is claimed to correct peripheral retinal image distortion. In our study, optic disc diameter was used as a unit of length, and adjustments for optic disc diameter were made during statistical analysis. Additionally, while UWF imaging provides a detailed view of the retinal periphery, other advanced imaging modalities such as optical coherence tomography (OCT) and adaptive optics (AO) might offer additional insights into the structural and functional changes associated with WDWP lesions. Fourth, previous literature has discussed WWOP and DWOP separately, but our observations using UWF imaging often show these conditions

appearing simultaneously, making them difficult to evaluate and distinguish. Therefore, we have combined them as WDWP for this study. Future research should refine the distinction between WWOP and DWOP for further analysis. Fifth, the age of myopia onset was not available for most patients, which may limit the interpretation of age-related trends. Lastly, it is important to note that the temporal quadrants are more easily imaged by the Optos system, which increases the likelihood that some lesions in other quadrants may have been missed. Long-term follow-up studies are needed to understand the natural history and progression of WDWP.

In conclusion, our study highlights that increased axial length is significantly associated with the occurrence and posterior localization of WDWP lesions. This finding suggests that axial elongation may play a crucial role in the development of these lesions, enhancing our understanding of WDWP in myopic eyes.

Abbreviations

AL	Axial Length
BCVA	Best-Corrected Visual Acuity
CHRPE	Congenital Hypertrophy of Retinal Pigment Epithelium
DD	Optic Disc Diameter
DWOP	Dark Without Pressure
ERM	Epiretinal Membrane
ICC	Intraclass Correlation Coefficient
ICL	Implantable Collamer Lens
IN	Inferior Nasal
IT	Inferior Temporal
LASIK	Laser-Assisted In Situ Keratomileusis
OCT	Optical Coherence Tomography
PRK	Photorefractive Keratectomy
SLO	Scanning Laser Ophthalmoscopy
SMILE	Small Incision Lenticule Extraction
SN	Superior Nasal
ST	Superior Temporal
UWF	Ultra-Widefield
UWFA	Ultra-Widefield Fluorescein Angiography
WDWP	White and Dark Without Pressure
WWOP	White Without Pressure

Acknowledgements
Not applicable.

Authors' contributions
SYC and CTP conceived and designed the study. HPL collected the data. SYC and CTP performed the statistical analysis. SYC drafted the manuscript. HPL and YGC contributed to data interpretation and critical revision of the manuscript. YGC supervised the entire study and served as the corresponding author. All authors read and approved the final manuscript.

Funding
This study received no specific grant from any funding agency in the public, commercial, or not-for-profit sectors.

Data availability
The datasets used and/or analyzed during the current study are available from the corresponding author on reasonable request. Due to the retrospective nature of the study and concerns regarding patient privacy, the data are not publicly available.

Declarations

Ethics approval and consent to participate
The study adhered to the tenets of the Declaration of Helsinki and was approved by the Medical Ethics Committee of Peking University Third Hospital (approval number: M2024275). Written informed consent was obtained from all participants.

Competing interests
The authors declare no competing interests.

Received: 27 December 2024 Accepted: 18 April 2025
Published online: 25 April 2025

References

1. Karlin DB, Curtin BJ. Peripheral chorioretinal lesions and axial length of the myopic eye. Am J Ophthalmol. 1976;81(5):625–35.
2. Pierro L, Camesasca FI, Mischi M, Brancato R. Peripheral retinal changes and axial myopia. Retina (Philadelphia, Pa). 1992;12(1):12–7.
3. Fawzi A, Nielsen J, Mateo-Montoya A, et al. Multimodal imaging of white and dark without pressure fundus lesions. Retina. 2014;34:2376–87.
4. Nagpal K, Goldberg MF, Asdourian G, et al. Dark-without-pressure fundus lesions. Br J Ophthalmol. 1975;59(9):476–9.
5. Shukla M, Ahuja OP. White with pressure (WWP) and white without pressure (WWOP) lesions. Indian J Ophthalmol. 1982;30(3):129–32.
6. Cheung R, Ly A, Katalinic P, et al. Visualisation of peripheral retinal degenerations and anomalies with ocular imaging. Semin Ophthalmol. 2022;37(5):554–82.
7. Nagiel A, Lalane RA, Sadda SR, Schwartz SD. Ultra-widefield fundus imaging: A review of clinical applications and future trends. Retina. 2016;36(4):660–78.
8. Ludwig CA, Moon J, Garg I, Miller JB. Ultra-widefield imaging for evaluation of the myopic eye. Semin Ophthalmol. 2021;36(4):185–90.
9. Yu G, Aaberg MT, Patel TP, et al. Quantification of retinal nonperfusion and neovascularization with ultrawidefield fluorescein angiography in patients with diabetes and associated characteristics of advanced disease. JAMA Ophthalmol. 2020;138(6):680–8.
10. Nguyen HTT, Hoang TT, Pham CM, et al. Prevalence and related factors of myopic retinopathy - a hospital-based cross-sectional study in Vietnam. Clin Exp Optom. 2023;106(4):427–30.
11. Yu H, Luo H, Zhang X, et al. Analysis of white and dark without pressure in a young myopic group based on ultra-wide swept-source optical coherence tomography angiography. J Clin Med. 2022;11(16):4830.
12. Patton N, Maini R, MacGillivary T, et al. Effect of axial length on retinal vascular network geometry. Am J Ophthalmol. 2005;140(4):648–53.
13. Kaneko Y, Moriyama M, Hirahara S, et al. Areas of nonperfusion in peripheral retina of eyes with pathologic myopia detected by ultra-widefield fluorescein angiography. Invest Ophthalmol Vis Sci. 2014;55(3):1432–9.
14. Singer M, Sagong M, van Hemert J, et al. Ultra-widefield imaging of the peripheral retinal vasculature in normal subjects. Ophthalmology. 2016;123(5):1053–9.
15. Oishi A, Hidaka J, Yoshimura N. Quantification of the image obtained with a wide-field scanning ophthalmoscope. Invest Ophthalmol Vis Sci. 2014;55(4):2424–31.
16. Nicholson L, Vazquez-Alfageme C, Clemo M, et al. Quantifying retinal area in ultra-widefield imaging using a 3-dimensional printed eye model. Ophthalmol Retina. 2018;2(1):65–71.
17. Thanos A, Todorich B, Pasadhika S, et al. Degenerative peripheral retinoschisis: Observations from ultra-widefield fundus imaging. Ophthalmic Surg Lasers Imaging Retina. 2019;50(9):557–64.
18. Lucente A, Taloni A, Scorcia V, Giannaccare G. Widefield and ultra-widefield retinal imaging: A geometrical analysis. Life. 2023;13(1):202.
19. Nicholson L, Vazquez-Alfageme C, Ramu J, et al. Validation of concentric rings method as a topographic measure of retinal nonperfusion in ultra-widefield fluorescein angiography. Am J Ophthalmol. 2015;160(6):1217-1225.e2.

20. Jonas JB, Bikbov MM, Wang YX, Jonas RA, Panda-Jonas S. Anatomic peculiarities associated with axial elongation of the myopic eye. J Clin Med. 2023;12(4):1317.
21. Gözüm N, Çakır M, Gücukoglu A, Sezen F. Relationship between retinal lesions and axial length, age, and sex in high myopia. Eur J Ophthalmol. 1997;7(3):277–82.
22. Khatwani N, Makhija S, Ahuja A. Clinical profile and distribution of peripheral retinal changes in myopic population in a hospital-based study in North India. Indian J Ophthalmol. 2022;70(4):1280–5.
23. Hunter JE. Retinal white without pressure: Review and relative incidence. Am J Optom Physiol Opt. 1982;59(4):293–6.
24. Akbani MI, Reddy KRK, Vishwanath K, Saleem M. Prevalence of peripheral retinal degenerations in the cases of myopia: A prospective study. Indian J Public Health Res Dev. 2014;5:58.
25. Orlin A, Fatoo A, Ehrlich J, et al. Ultra-widefield fluorescein angiography of white without pressure. Clin Ophthalmol. 2013;7:959–64.
26. Al-Sheikh M, Phasukkijwatana N, Dolz-Marco R, et al. Quantitative OCT angiography of the retinal microvasculature and the choriocapillaris in myopic eyes. Invest Ophthalmol Vis Sci. 2017;58(4):2063–9.
27. dell'Omo R, Cifariello F, dell'Omo E, et al. Retinal microvasculature in patients with epiretinal membrane evaluated by optical coherence tomography angiography. Retina. 2021;41(7):1397–406.
28. Diaz RI, Sigler EJ, Randolph JC, et al. Spectral domain optical coherence tomography characteristics of white-without-pressure. Retina. 2014;34:1020–1.
29. Nagpal KC, Goldberg MF, Rabb MF. Ocular manifestations of sickle hemoglobinopathies. Surv Ophthalmol. 1976;20(5):391–411.

Publisher's Note